Title
Covarying structural alterations in laterality of the temporal lobe in schizophrenia: A case for source-based laterality.

Journal
NMR in biomedicine, 33(6)

ISSN
0952-3480

Authors
DeRamus, Thomas P
Silva, Rogers F
Iraji, Armin
et al.

Publication Date
2020-06-01

DOI
10.1002/nbm.4294

Peer reviewed

Received: 10 January 2020 | Revised: 21 February 2020 | Accepted: 24 February 2020
DOI: 10.1002/nbm.4294

RESEARCH ARTICLE

NMR IN BIOMEDICINE WILEY

Covarying structural alterations in laterality of the temporal lobe in schizophrenia: A case for source-based laterality

Thomas P. DeRamus[1] | Rogers F. Silva[1] | Armin Iraji[1] | Eswar Damaraju[1] | Aysenil Belger[2] | Judith M. Ford[3] | Sarah C. McEwen[4] | Daniel H. Mathalon[3] | Bryon A. Mueller[5] | Godfrey D. Pearlson[6,7] | Steven G. Potkin[8] | Adrian Preda[8] | Jessica A. Turner[1,9] | Jatin G. Vaidya[10] | Theo G. M. van Erp[8] | Vince D. Calhoun[1,6,9,11]

[1]Tri-institutional Center for Translational Research in Neuroimaging and Data Science (TReNDS), Georgia State University, Georgia Institute of Technology, Emory University, Atlanta, Georgia, USA

[2]Department of Psychiatry, University of North Carolina Chapel Hill, North Carolina, USA

[3]Department of Psychiatry, University of California San Francisco, San Francisco, California, USA

[4]Pacific Neuroscience Institute Foundation, Santa Monica, California, USA

[5]Department of Psychiatry, University of Minnesota, Minneapolis, Minnesota, USA

[6]Department of Psychiatry, Yale University School of Medicine, New Haven, Connecticut, USA

[7]Olin Neuropsychiatry Research Center, Institute of Living, Hartford, Connecticut, USA

[8]Department of Psychiatry and Human Behavior, University of California Irvine, Irvine, California, USA

[9]Department of Psychology, Georgia State University, Georgia, USA

[10]Department of Psychiatry, University of Iowa, Iowa, USA

[11]Department of Electrical and Computer Engineering, Georgia Tech, Georgia, USA

Correspondence
T.P. DeRamus, Tri-institutional Center for Translational Research in Neuroimaging and Data Science (TReNDS), Georgia State University, Georgia Institute of Technology, Emory University, Atlanta 30303, Georgia, USA.
Email: tderamus@gsu.edu

Funding information
National Institute of Biomedical Imaging and Bioengineering, Grant/Award Numbers: R01EB006841, R01EB020407; National Institute of General Medical Sciences, Grant/Award Numbers: P20GM103472, P30GM122734; National Institute of Mental Health, Grant/Award Number: R01MH094524; National Science Foundation, Grant/Award Number: 1539067

The human brain is asymmetrically lateralized for certain functions (such as language processing) to regions in one hemisphere relative to the other. Asymmetries are measured with a laterality index (LI). However, traditional LI measures are limited by a lack of consensus on metrics used for its calculation. To address this limitation, source-based laterality (SBL) leverages an independent component analysis for the identification of laterality-specific alterations, identifying covarying components between hemispheres across subjects. SBL is successfully implemented with simulated data with inherent differences in laterality. SBL is then compared with a voxel-wise analysis utilizing structural data from a sample of patients with schizophrenia and controls without schizophrenia. SBL group comparisons identified three distinct temporal regions and one cerebellar region with significantly altered laterality in patients with schizophrenia relative to controls. Previous work highlights reductions in laterality (ie, reduced left gray matter volume) in patients with schizophrenia compared with controls without schizophrenia. Results from this pilot SBL project are the first, to our knowledge, to identify covarying laterality differences within discrete temporal brain

Abbreviations used: BIRN, biomedical informatics research network; BOLD, blood oxygen-level dependence; CON, participants without schizophrenia; EBM, entropy-bound minimization; FDR, false discovery rate; FWHM, full width half-maximum; INU, intensity nonuniformity; IVA, independent vector analysis; LI, laterality index; MRN, mind research network; MTG, middle temporal gyrus; NICIrvine, Neuroimaging Center of University of California Irvine; NITRC, neuroimaging tools and research collaborator; PANSS, positive and negative syndrome scale for schizophrenia; PCA, principle component analysis; SBL, source-based laterality; SNC, structural network connectivity; STG, superior temporal gyrus; SZ, participants with schizophrenia; UCIrvine, University of California Irvine; UCLA, University of California Los Angeles; UIowa, University of Iowa; UMCMRR, University of Minnesota Medical School's Center for Magnetic Resonance Research; VBM, voxel-based morphometry.

regions. The authors argue SBL provides a unique focus to detect covarying laterality differences in patients with schizophrenia, facilitating the discovery of laterality aspects undetected in previous work.

KEYWORDS

brain laterality, independent component analysis, schizophrenia, voxel-based morphometry

1 | INTRODUCTION

Alterations of gray matter in patients with schizophrenia (SZ) have been frequently reported in studies analyzing functional and structural MRI data and meta-data.[1–10] Many of these alterations are weighted towards the left hemisphere, leading researchers to suggest schizophrenia may produce alterations in brain laterality in SZ compared with controls with no diagnosis of schizophrenia (CON).[10–23] However, many of the findings upon which this hypothesis is based center on the outcome of regional or whole-brain voxel/vertex-based methods, which may not be ideal for assessing laterality-specific conclusions. Traditionally, such changes can be assessed by calculating a single laterality index (LI) for each subject, using Equation 1:

$$LI = f\frac{Q_{LH} - Q_{RH}}{Q_{LH} + Q_{RH}} \tag{1}$$

where *Q is* the quantity of the MRI metric of interest (eg, blood oxygen-level dependence [BOLD] percent signal change, gray matter volume, cerebral blood-flow volume), *LH* and *RH* represent *Q* for the left and right hemisphere, respectively, and *f* represents a scaling factor, usually 1 or 100,[24–27] with positive values indicating left-hemispheric dominance and negative values indicating right-hemispheric dominance. Many toolboxes are available to calculate the LI of neuroimaging data[28,29] utilizing this formula. Unfortunately, the laterality calculation itself has limitations.

One of the most notable limitations of the LI calculation is a lack of consensus on what metric should be used for *Q*, with suggestions including voxel intensity,[24,26] weighted sums,[30] mean signal change,[31,32] average correlation coefficients,[33] *F*-values,[34] *t*-values[35,36] and weighted *t*-values[37–39] in isolation or which survive certain thresholds.[27] The use of *t*-values is problematic because negative *t*-values can lead to significant misinterpretations of the output (which can be mitigated by using absolute values).[27,40] Furthermore, whole-brain versus region of interest (ROI) approaches may yield very different results based on ROI selection and thresholding.[27] Thresholds within specific ROIs may not be appropriate for some populations in which these functions are altered or have shifted (eg, stroke, tumor), while whole-brain analyses may lack the ability to identify specific brain regions or patterns of variation across multiple brain regions. Additionally, researchers often choose to omit the cerebellum from laterality analyses due to contralateral connections of the cerebellum and cortex biasing LI measures.[27,39,41–43] Ironically, the advantages of ROI and/or cluster/vertex wise analyses are also their greatest flaws. For example, while ROI-based approaches (such as those implemented in *Freesurfer*[44–51] and similar packages) produce stable results with larger effect sizes in populations where differences may be focal or variable (ie, hand regions of the primary motor cortex in piano players vs. nonpiano players), differences may vanish when values are averaged over unnecessarily large ROIs.[52,53] This risk considerably increased when large smoothing kernels were applied to the data (see Scarpazza et al for a brief review).[54] In addition, such analyses risk considerable reductions in power relative to the number of ROIs, as multiple comparisons or models would need to be performed for each ROI or ROI pair. While *Freesurfer*[44,46–51] is capable of vertex-wise corrections within masks (see http://freesurfer.net/fswiki/BuildYourOwnMonteCarlo for documentation and Patriquin et al[55] for an example of implementation) as opposed to ROIs from atlases, this approach rarely seems to be used. However, even when voxel/vertex-wise analyses are implemented, the choice of correction and sample size could lead to vastly different results between studies due to the power requirements for voxel/cluster wise corrections.[27,56–59] As such, ROI and voxel agnostic methods would significantly improve laterality inferences in MRI data.

Our goal in this work was to develop an improved measure of laterality which exhibits (1) agnosticism regarding to the size/shape/cluster extent of a region, (2) laterality-specific pattern identification rather than region-specific identification and (3) robustness to patterns of alteration in the absence of a priori regions. To that end, the authors propose a novel solution to analyzing laterality by directly estimating covarying networks from homotopic mirror images via Independent Component Analysis (ICA), called source-based laterality (SBL). SBL is an extension of source-based morphometry (SBM), which utilizes a multivariate, ICA-based approach to identify interrelationships across voxels in anatomical analyses such as gray matter maps in voxel-based morphometry.[60] In lieu of utilizing a gray matter map, SBL utilizes a homotopic subtraction of right and left voxels from gray matter hemispheres, implemented by flipping the right hemisphere and subtracting it from the left, producing a single, voxel-wise difference image between the two hemispheres. The resulting hemispheric difference image for each participant is then analyzed across participants using spatial ICA. In this manner, ICA solutions are specific to laterality-based components which covary between hemispheres

across subjects. The authors argue SBL provides a unique approach to detecting covarying laterality differences between SZ and CON individuals, enabling researchers to capture subtle alterations in cortical symmetry that are not identified by traditional voxel- or ROI-based approaches.

As a proof of concept, a simulation of gray matter difference maps is used to demonstrate the robustness in the identification of spatial covarying patterns using SBL. SBL is then applied to difference images of gray matter volume maps from SZ and CON within the function biomedical informatics research network (FBIRN).[61,62] The authors hypothesize gray matter difference images leveraged by SBL will identify alterations in structural gray matter laterality in SZ compared with CON (demonstrated in previous literature[2–6,8–10,13–23,63–72]) and structural network covariance (SNC) while retaining spatial specificity and statistical power unavailable to voxel- or ROI-based approaches.

2 | METHODS

2.1 | Simulation

2.1.1 | Data generation

Step 1 included the generation of a 400 x 400 2D images with 1 mm^2 dimensions containing three asymmetric ROIs (ROI 1 area = 2188 mm^2, ROI 2 area = 757 mm^2, ROI 3 area = 347 mm^2) to serve as sources. Step 2 included source generation, with source 1 (ROI 1) consisting of an inverse hyperbolic tangent transformation of a normally distributed vector of 2188 values centered on a mean of 0 with a standard deviation of 0.27, with 0.5 added as a constant. Source 2 (including ROIs 2 and 3) also consisted of an inverse hyperbolic tangent transformed vector with an added constant of 0.5, but of 1104 values with a mean of 0 and a standard deviation of 0.4, all of which were multiplied by a value of 0.1. Gaussian noise was generated across the remaining values in the image mask using a normal distribution centered at a mean of 0 and a standard deviation of 0.15. Example images produced with this process are displayed in Figure 1. Step 3 generated 300 2D images with the specified source parameters, with 150 representing "controls" and 150 representing "patients". For each simulated control, weights for source 1 were chosen randomly from values between 0.5-0.8 and 0.2-0.4 for source 2. For each simulated patient, weights for source 1 were randomly chosen between 0.2-0.4 and 0.8-1 for source 2. Finally, ground truth weights were recorded for each source to assess the accuracy of the SBL component weightings.

2.1.2 | SBL

SBL was performed on the 300 simulated subtraction maps implemented within the group ICA of fMRI toolbox (GIFT; http://mialab.gsu.edu/software/gift)[73] utilizing group-level principle component analysis (PCA), spatial ICA with infomax, and calculation of individual spatial maps using PCA-based back-reconstruction to identify three independent components, resulting in loading parameters for each component in the simulated group data.[60]

2.2 | Real data

2.2.1 | Demographic information

T1 weighted images from 326 participants, 167 SZ (male/female: 129/38) and 159 (male/female: 113/46) CON from seven imaging centers: the Mind Research Network (MRN), Duke University, University of California Los Angeles (UCLA), University of California Irvine (UCIrvine), Neuroimaging Center of University of California Irvine (NICIrvine), University of Iowa (UIowa), and the University of Minnesota Medical School's Center for Magnetic Resonance Research (UMCMRR). Participants provided informed consent in accordance with institutional review board requirements of each participating university. The Edinburgh Handedness Inventory (EHI)[74] was collected to assess the dominant hand from each participant as an additional variable of consideration when assessing laterality. Briefly, the EHI scores responses regarding hand use for 10 different tasks, and assigns ambidexterity, left, or right hand dominance based on the decile from the totaled hand use during each task.[74] The scale ranges from −100 (completely left dominant) to +100 (completely right dominant), with a median of $-28 \leq LI < 48$ indicating ambidexterity.[74] An interactive example of the questionnaire can be found at the Organization for Human Brain mapping at http://www.brainmapping.org/shared/Edinburgh.php. Detailed descriptions of data processing, storage protocols and participant anonymization can be accessed at the main FBIRN portal on neuroimaging tools and research collaboratory (NITRC) at https://www.nitrc.org/projects/fbirn/, or queried directly through http://schizconnect.org following registration. BIRN protocols designate identifying information (ie, gender, age, subject ID, etc.), which cannot be directly shared without registering with the BIRN initiative.

SZ did not display significant differences between controls on age (18-68 years, mean = 38.19 ± 11.39 years, W = 14169, P = 0.29, gender composition (χ^2 = 1.3176, P = 0.25) or handedness (χ^2 = 1.9454, P = 0.39 [Monte-Carlo w/2 k]). These statistics are summarized in Table 1. Site-

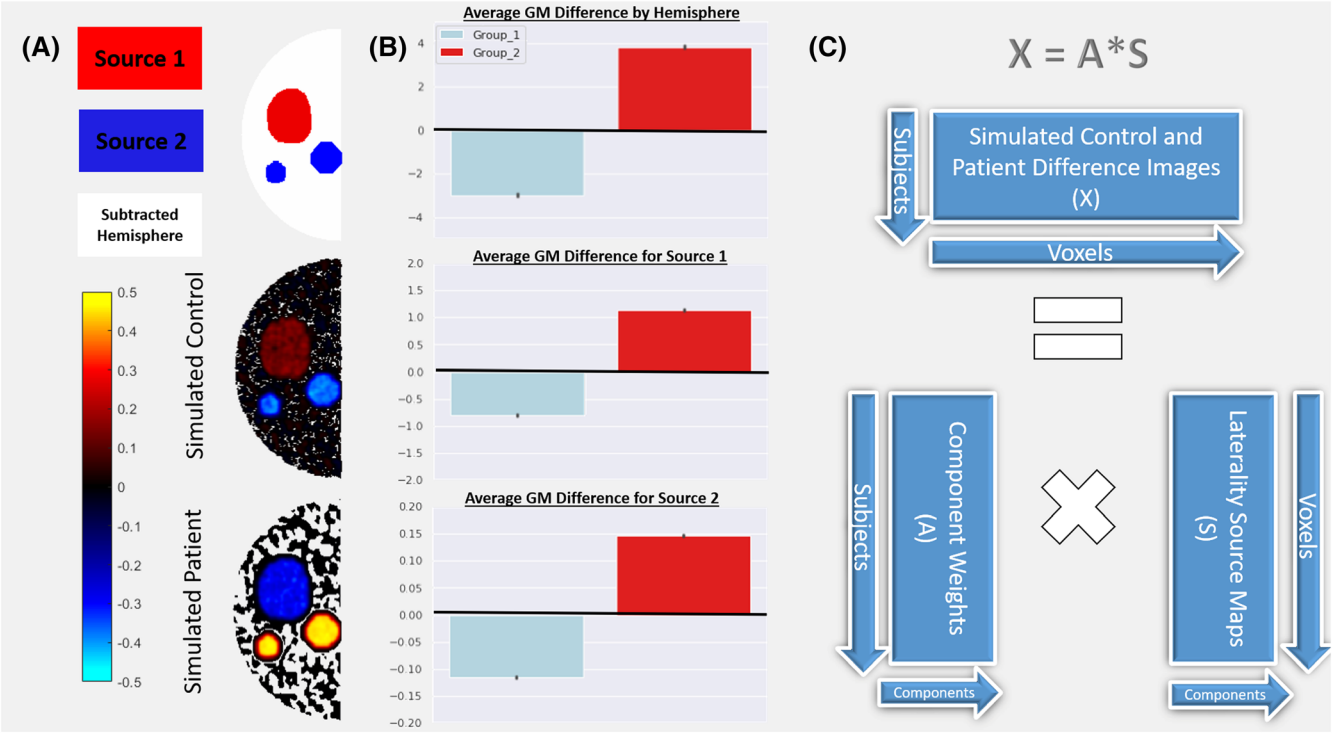

FIGURE 1 (A) Top figure: simulated source 1 (single sphere, red) and source 2 (double sphere, blue). Bottom two figures: for controls (middle) source 1 is primarily positive while source 2 is primarily negative. For patients (bottom) intensities are negative for source 1 and positive for source 2. Intensities for raw laterality images are bound between 0.5 and −0.5 for visualization. (B) Average difference maps by group are displayed for the left hemisphere (top figure), source 1 (middle figure) and source 2 (bottom figure). Values above 0 (black line) indicate greater volume in the left hemisphere, while values below 0 indicate greater gray matter (GM) volume in the right hemisphere. (C) Breakdown of independent component analysis utilizing the formula X[data] = A[Mixing Matrix] * S[Source Matrix]. Simulated difference images (X) are provided and decomposed into component weights (A) and a source matrix (S)

TABLE 1 Participant demographic information and comparisons

	SZ	Typical controls	Test statistic	*P*-value
Age range, years	18-62	19-60	*W* = 14169	0.29
Male/female	129/38	113/46	$\chi 2$ = 1.32	0.25
Handedness R/L/A	152/11/4	151/6/2	$\chi 2$ = 1.95	0.39
Median PNASS Negative	14		Range: 7-39	
Median PNASS Positive	14		Range: 7-33	

*Indicates statistical significance at or below the 0.05 level.
W represents the rank-difference statistic from a Wilcoxon rank-sum test.
χ^2 Represents the goodness-of-fit from a Pearson chi-squared test.

wise differences in participant gender approached significance (χ^2 = 11.9, df = 6, *P* = 0.06), but no significant differences in the representation of diagnostic groups (χ^2 = 1.07, df = 6, *P* = 0.98) were present.

2.2.2 | Image parameters and quality analyses

High-resolution T1 Siemens MP-RAGEs were collected from 284 patients on six 3 T Siemens Tim Trio Systems (MRN, UCLA, UCIrvine, NICIrvine, UMCMRR and UIowa). MP-RAGE parameters were TR/TE/TI = 2300/2.94/1100 ms, flip angle = 9°, resolution = 256 × 256 × 160. The remaining 42 T1 images were acquired using a 3 T General Electric (GE) Discovery MR750 scanner using a GE IR-SPGR sequence (TR/TE/TI = 5.95/1.99/450 ms, flip angle = 12°, resolution = 256 × 256 × 166). Images from all sites covered the entire brain with field of view

(FOV) = 220 mm^2, with 324 of the scans utilizing voxel dimensions = 0.86 × 0.86 × 1.2 mm^3, with one scan using dimensions = 0.9 × 0.9 × 1.2 mm^3 and one using 1mm^3 isometric voxels. All scans utilized the sagittal scan plane, GRAPPA/ASSET acceleration factor = 2, and the number of excitations = 1.

2.2.3 | CON versus SZ

Image quality metrics on each participant were calculated using virtual python 3.6 environment of *MRIQC* 0.11.0.[75] Group comparisons revealed significant differences between SZ and CON in the coefficient of joint variation (W = 15 940, P = 0.002, r = 0.17), higher contrast-to-noise ratio $t_{(322.62)}$ = −3.7636, P = 0.0002, d = −0.42, higher average data smoothness (FWHM) (W = 11 471, P = 0.03, r = 0.11) and greater intensity nonuniformity parameters (INU) $t_{(318.46)}$ = −3.9682, P < 0.0001, d = −0.44, CI 95%: −0.07-0.02 in controls compared with SZ, but higher entropy focus criterion $t_{(322.9)}$ = 4.39, P < 0.0001, d = 0.48, CI 95%: 0.01-0.03, gray matter residual partial volume error, $t_{(324)}$ = 2.69, P = 0.007, d = 0.30, CI 95%: 0.15-0.61, white matter maximum intensity ratio (W = 11 474, P = 0.03, r = 0.12), and initial International Consortium of Brain Mapping asymmetric tissue probability map overlap (W = 7745, P < 0.001, r = 0.36) were found in SZ compared with controls. However, no significant differences between patients and controls in gray matter signal-to-noise ratio (W = 12 742, P = 0.5) were found. These results are summarized in Figure S1.

2.2.4 | Comparisons by data acquisition site

Site-wise analyses of image quality metrics identified differences on coefficient of joint variation, Kruskal-Wallis χ^2 = 91.175, df = 6, P < 0.001, gray matter signal-to-noise ratio $F(6, 319)$ = 39.81, P < 0.001, $\acute{\omega}^2$ = 0.42, entropy focus criterion, $F(6, 319)$ = 39.81, P < 0.001, $\acute{\omega}^2$ = 0.32, INU correction parameters Kruskal-Wallis χ^2 = 111.46, df = 6, P < 0.001, and average smoothness Kruskal-Wallis χ^2 = 129.37, df = 6, P < 0.0001. However, no significant differences were found for contrast-to-noise ratio, gray matter residual partial volume error, or overlap with the initial ICBM asymmetric tissue probability map. These comparisons are also summarized in Figure S2 a-e.

2.3 | Image processing and analysis

Gray matter volume maps were computed from all T1 images using the SPM12 voxel-based morphometry "new segmentation" pipeline (build 6906).[76–78] The pipeline includes segmentation based on priors for six tissue classes, normalization to the MNI 152 template, and modulation of gray matter maps the Jacobian determinant to preserve tissue volume. Once processed through SPM, gray matter maps were smoothed with a 10 mm FWHM Gaussian kernel. Gray matter maps were then reregistered from the asymmetric template in SPM to a symmetric MNI template in FSL[79,80] version 6.0.0 using ANTs[81,82] with nearest neighbor interpolation. Following smoothing and renormalization, each map was mirrored using AFNI's (version AFNI_18.3.01)[83] *3dLRflip* and the mirror was subtracted from the original smoothed image, then a mask of all positive values of x (left hemispheric) was applied to the difference image to generate a laterality map.

2.3.1 | Voxel-wise analysis

The laterality map computed using difference images were analyzed using voxel-based morphometry implemented in SPM12 (version 7487). Ordinary least-squares regression was performed at each voxel with the following factors: diagnosis (CON vs. SZ), gender (male vs. female), handedness (right, left, ambidextrous) and site of data acquisition. Comparisons between CON and SZ were computed on the residuals with all other factors treated as nuisance regressors.

2.3.2 | SBL

Previous SBL work in whole-brain information from the same data utilized Akaike's information criterion[84] to suggest a 30-component model for source based morphometry analysis.[60] As such, a similar 30-component solution was computed from the 326 laterality maps utilizing entropy-bound minimization (EBM)-ICA,[85] an algorithm which is able to capture more flexible source distributions (eg, sub-Gaussian, symmetric or skewed) compared with approaches like infomax[86,87] and selection of the best run from 20 runs for component stabilization.

2.3.3 | Multiple regression

Component weights that were visually identified as local to gray matter were regressed onto diagnostic status (SZ vs. CON), handedness, and data acquisition site. The 30 regressions were multiple comparison-corrected using a 5% false discovery rate (FDR).[88]

2.3.4 | Clinical correlations

Weights from SZ were extracted from components associated with diagnostic status. Spearman's ρ partial correlations across diagnosis-specific components were performed with positive, negative and total positive and negative syndrome scale (PANSS)[89] to probe brain/behavior relationships in SZ.

2.3.5 | SNC calculations

Mixing matrices for components associated with diagnostic status totaling six comparisons were correlated with one another to measure the inter-relationship between covarying networks, or SNC, using a partial correlation to account for data acquisition site. Contrasts were adjusted for multiple comparisons using a Holm correction,[90] as an FDR of 5% for six comparisons is not an integer (0.03) to examine relationships between components.

3 | RESULTS

3.1 | Toy example

The GIFT ICA pipeline generated three components as anticipated. These included: component 1 (which was resembled source 2), component 2 (which resembled source 1) and a third component labeled as noise due to its appearance (see Figure 2). Images displaying the components from the simulated data are summarized in Figure 2. Comparisons of loading parameters for the simulated CON versus SZ groups identified a significantly greater ($W > 0$, $P < 0.0001$, $r = 0.865$) component weightings for component 1 (source 2) in simulated CON (median = 0.98) compared with simulated SZ (median = −0.995). The opposite relationship was apparent in component 2 (source 1), with simulated CON exhibiting significantly greater ($W = 22500$, $P < 0.0001$, $r = 0.865$) median component weights (median = 0.99) compared with simulated CON (median = −0.99).

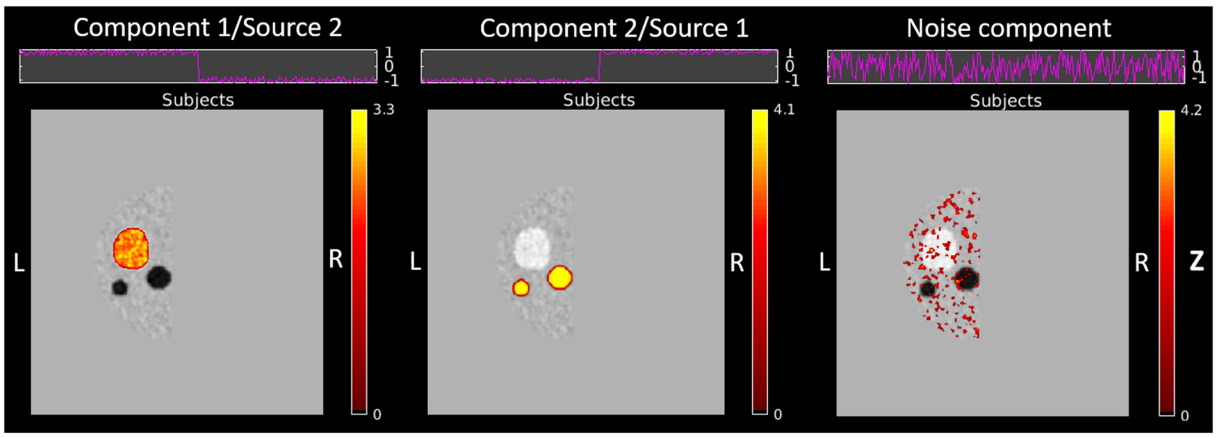

FIGURE 2 Component estimations resolved from SBL on simulated data. The estimation of source 1 (left) has a distribution and appearance and distribution similar to source 1. The component estimated for source 2 (middle) similarly has a distribution and appearance nearly identical to source 2, also occurring across multiple regions. The third estimation (right) represents a component estimated from sections of Gaussian noise generated as part of the simulated data

3.1.1 | Voxel-wise analysis on laterality maps

No voxels survived a 5% voxel-wise FDR[88] correction ($t_{(316)}$ = 4.814, k = 14.22). If the cluster extent threshold is removed, a small number of subcortical and frontal regions are present, but theresults appear in regions associated with dura and cerebrospinal fluid and are likely artifacts. See Figure 3 for uncorrected image results.

3.1.2 | SBM component analysis of laterality maps

Each of the 30 components from the SBM was visually inspected to flag components as "possible source" or "possible artifact". The former category included regions within the cortical mask, while the latter category included ringing around the mask and the inclusion of noncortical regions. No components exhibited patters defined as "possible artifact", so loadings from all 30 components were retained for subsequent analyses. An interactive image in html constructed with *papaya* (build 782a193, https://rii-mango.github.io/Papaya/) may be found in the supporting information (Supplementary Material 1). Of the 30 performed regressions, 10 of the models reached statistical significance after a 5% FDR correction for multiple comparisons. However, only four of the component weights (components 7, 16, 28 and 30) were significantly influenced by participant diagnostic status (CON vs. SZ). Components significantly related to diagnosis are displayed in Figure 4A, while contrasts are displayed in Figure 4B. F-values, P and corrected P values, adjusted R^2 and partial omega squared values for each are summarized in Table 2. Post hoc Wilcoxon rank-sum tests[91] identified significantly greater cerebellar component weights in CON participants compared to participants with SZ (W = 16216, P < 0.001, r = 0.19, CI 95%: 0.17-0.57), but significantly reduced weights in CON participants compared participants with SZ in STG components (W = 11 586, P < 0.05, r = 0.11, CI 95%: −0.45-0.003), STG/MTG/postcentral components (W = 11416, P < 0.03, r = 0.12, CI 95%: −0.44-0.03) and MTG components (W = 10357, P < 0.001, r = 0.19, CI 95%: −0.61-0.17). Component spatial maps were thresholded at a Z score of 3 (displayed in Figure 4A) and average difference scores for laterality maps for each subject were compared. Differences reflected those displayed by component weights, with CON displaying right laterality and SZ displaying left laterality. It should be noted that the weights from component 7 suggest an increase in CON and a reduction in SZ, but the degree to which right lateralization is present in CON is greater than the degree of left lateralization in SZ. Weights for components 16, 28 and 30 similarly mirror mean distributions, in which CON display reduced weights compared with SZ, but this is relative to right lateralization (expressed as negative numbers). The ICA-based approach highlights the relationship between the two groups agnostic to the direction.

3.2 | Correlations with clinical measures

Partial Spearman ρ correlations accounting for site of data acquisition did not reveal any significant relationship between components for total positive or general total PANSS scores. One statistically significant negative correlation between total negative PANSS symptoms and component 7 was identified, which survived a Holm[90] correction for multiple comparisons (ρ = −0.20, P = 0.009, *Holm-P* = 0.03). When extracting average gray matter volumes relative to the component, this translates to an increase in right lateralization (negative values) associated with less negative symptoms in SZ. No other statistically significant relationships were identified for components 16, 28 and 30 with PANSS negative symptoms scores. The relationship is described in a Spearman plot generated using the *fifer* (version 1.1) package in *R*[92] (see Figure 5).

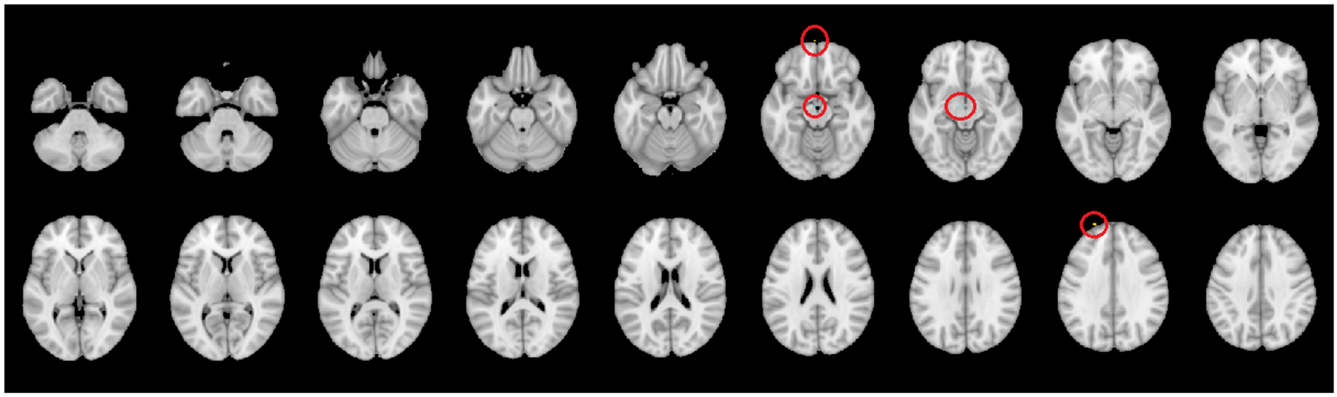

FIGURE 3 Statistically significant voxels after a 5% FDR correction ($t_{(314)}$ = 4.861), with no cluster thresholding (k = 0). Warm colors indicate CON > SZ, while cool colors indicate SZ > CON. The model used for this analysis treats age, gender, handedness and data acquisition site as nuisance variables. Results are flagged with red circles for visualization

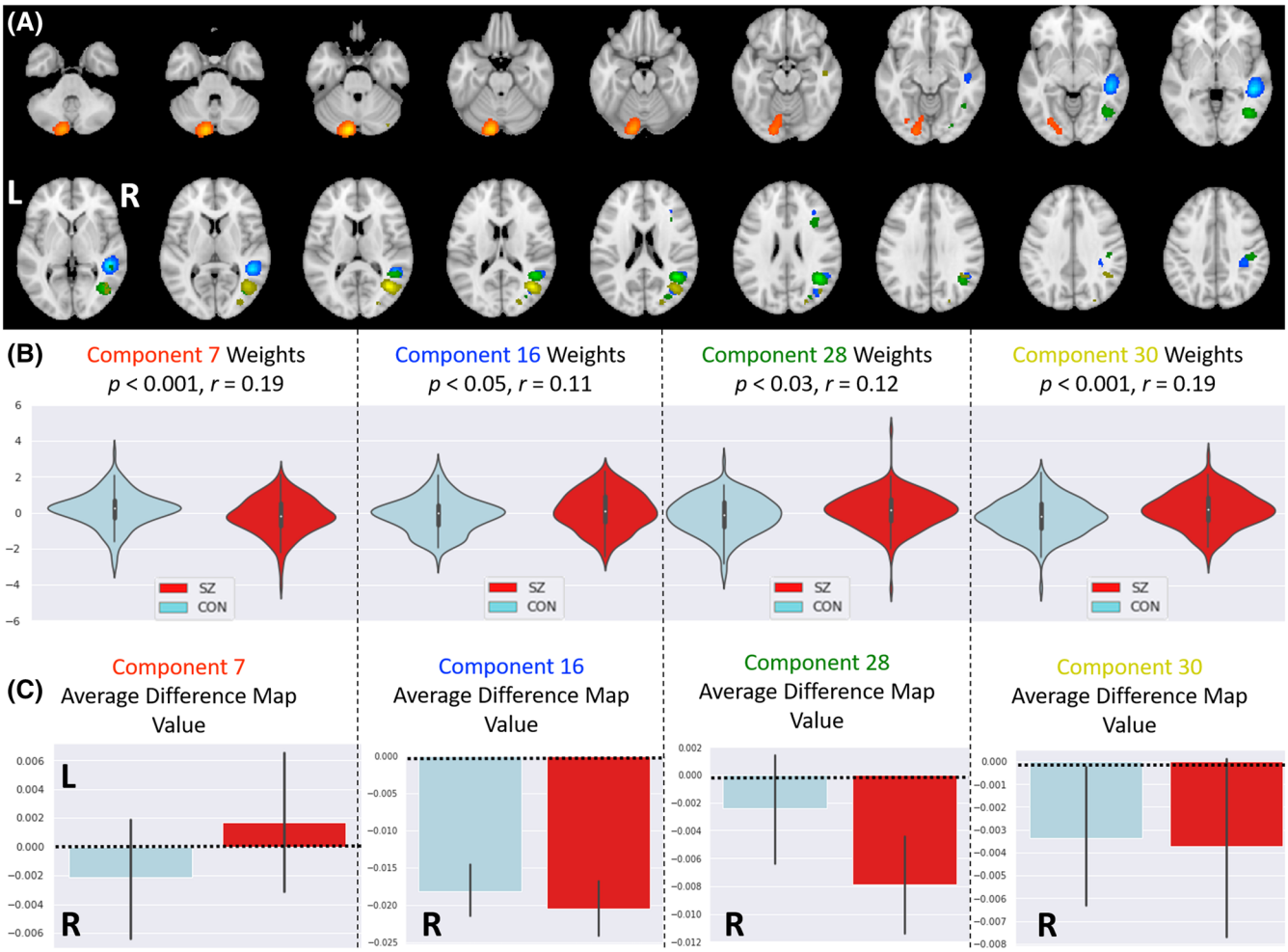

FIGURE 4 (A) Components significantly associated with CON (blue) versus SZ. These include component 7 (red/cerebellum), 16 (blue/superior temporal), 28 (green/postcentral, superior and middle temporal) and 30 (yellow/middle temporal). (B) SZ (red violin) displayed significantly lower weightings in component 7 compared with CON (blue violin), but SZ displayed significantly greater weightings in components 16, 28 and 30 compared with CON. (C) Average difference score for thresholded (Z = 3) components. Zero on the graph is indicated by a dotted line. Positive values indicate greater gray matter volume in left hemisphere (L), while negative values indicate greater gray matter volume in the right (R) hemisphere. For component 7, SZ exhibit greater left hemispheric gray matter, while CON exhibit right laterality. For components 16, 28 and 30, gray matter is larger in the right hemisphere, but the volume is significantly increased in SZ compared with CON. Hemispheric displays are organized relative to SZ

3.3 | Structural SNC

Pearson correlations between the mixing matrices from components 7, 16, 28 and 30 identified a significant negative relationship between component 7 and component 30 which survived a Holm correction[90] for multiple comparisons ($r = -0.2$, *Holm-P* = 0.002). Significant uncorrected correlations between components 16 and 28 with component 30 were identified ($r = 0.12$, $P = 0.03$ and $r = -0.17$, $P = 0.03$, respectively), but these results did not survive correction for multiple comparisons (*Holm-P* = 0.13). A nodal illustration of the structural SNC matrix with nodal connections is displayed in Figure 6.

4 | DISCUSSION

We demonstrate a novel approach to assess structural laterality within the brain. SBL provides advantages over traditional approaches to studying brain laterality in that it does not require a priori selection of an ROI, preserves spatial information within the data, and identifies covarying patterns of laterality alterations in lieu of potentially skewed voxel-wise quantifications which identify differences irrespective of covariation in

TABLE 2 Linear regression results by component

Component	F (9,317)	F P-value	FDR P-value	Adj. R^2	Significant predictor(s)	Predictor t-value	Predictor p-value	$_p\hat{\omega}^2$	Assumption tests P-values: Heteroscedasticity	Nonnormal residuals	Autocorrelated residuals
1	1.79	0.070	0.175	0.021					0.528	0.701	0.996
2	0.95	0.484	0.660	−0.001					0.355	0.355	0.452
3	0.77	0.649	0.778	−0.007					0.724	0.723	0.358
4	1.40	0.187	0.318	0.011					* <0.001	* <0.001	0.986
5	3.51	*<0.001	*0.003	0.065					0.639	0.026	0.928
					Site ID/(Duke)	4.31	<0.001	0.071			
6	2.33	*0.015	*0.045	0.036					*0.03	0.705	*0.006
					Site ID/(Duke)	2.35	<0.001	0.036			
7	2.80	*0.004	*0.012	0.047					0.375	* <0.001	0.534
					Diagnostic status (SZ vs. CON)	3.57	<0.001	0.033			
					Handedness (left)	2.06	0.040	0.015			
8	0.55	0.834	0.863	−0.013					0.765	*0.006	0.836
9	1.35	0.210	0.332	0.010					0.338	0.096	*0.032
10	0.91	0.519	0.677	−0.003					0.741	0.893	0.24
11	7.90	* <0.001	* <0.001	0.161					0.438	*0.031	*0.004
					Site ID/(Duke)	−5.82	<0.001	0.158			
					Site ID/(MRN)	1.97	0.050	0.158			
12	1.39	0.191	0.318	0.011					0.932	0.562	0.432
13	1.22	0.284	0.426	0.006					0.623	* <0.001	0.892
14	4.34	* <0.001	* <0.001	0.085					0.818	0.136	0.546
					Site ID/(Duke)	4.34	<0.001	0.086			
					Site ID/(UCLA)	2.27	0.024	0.086			
15	1.40	0.189	0.318	0.011					0.98	0.178	0.608
16	8.42	* <0.001	* <0.001	0.171					0.657	0.22	0.968
					Diagnostic status (SZ vs. CON)	−2.27	0.024	0.012			
					Handedness (ambidextrous)	−1.99	0.047	0.015			
					Site ID/(Duke)	−5.84	<0.001	0.151			
17	2.98	*0.002	*0.009	0.052					*0.003	*0.027	0.618
					Site ID/(MRN)	3.80	<0.001	0.053			

(Continues)

TABLE 2 (Continued)

Component	F (9,317)	F P-value	FDR P-value	Adj. R^2	Significant predictor(s)	Predictor t-value	Predictor p-value	$_p\acute{\omega}^2$	Assumption tests P-values: Heteroscedasticity	Nonnormal residuals	Autocorrelated residuals
					Site ID/(NIClrvine)	2.28	0.024	0.053			
					Site ID/(UClrvine)	2.04	0.042	0.053			
					Site ID/(UCLA)	2.94	0.004	0.053			
					Site ID/(UI)	2.85	0.005	0.053			
18	0.87	0.554	0.693	−0.004					0.261	0.278	0.384
19	2.03	0.036	0.098	0.028					0.51	0.505	0.272
20	0.68	0.731	0.812	−0.009					0.349	0.12	0.926
21	0.32	0.970	0.970	−0.019					0.762	*0.004	0.642
22	0.61	0.785	0.841	−0.011					0.297	0.113	0.636
23	2.87	*0.003	*0.011	0.049					0.445	0.496	0.17
					Site ID/(UCLA)	2.60	0.010	0.038			
24	1.62	0.109	0.219	0.017					0.421	0.121	0.404
25	1.62	0.110	0.219	0.017					0.886	*0.041	0.078
26	0.73	0.677	0.781	−0.007					0.746	0.16	0.232
27	1.75	0.078	0.179	0.020					0.603	0.096	0.734
28	3.04	*0.002	*0.008	0.053					0.309	* <0.001	0.35
					Diagnostic status (SZ vs. CON)	−2.31	0.021	0.014			
					Site ID/(MRN)	2.92	0.004	0.046			
					Site ID/(UClrvine)	2.23	0.026	0.046			
29	1.05	0.398	0.568	0.001					0.829	0.218	*0.008
30	3.29	* <0.001	*0.005	0.060					0.418	0.257	*0.05
					Diagnostic status (SZ vs. CON)	−3.58	<0.001	0.035			
					Site ID/(Duke)	3.14	0.002	0.032			
					Site ID/(MRN)	2.24	0.026	0.032			

Abbreviations: CON, control participant without a diagnosis of schizophrenia; Duke, Duke University; MRN, Mind Research Network; NIUClrvine, Neuroimaging Center of University of California Irvine; SZ, participant with a diagnosis of schizophrenia; UClrvine, University of California Irvine; UCLA, University of California Los Angeles; UI, University of Iowa.

*Indicates statistical significance at or below the 0.05 level. $_p\acute{\omega}^2$ values are calculated by independent variable (eg, diagnosis, data collection site), not by the factor in which dummy variables for each category has been coded. We present the $_p\acute{\omega}^2$ for the entire independent variable with the factor of interest for ease of visualization.

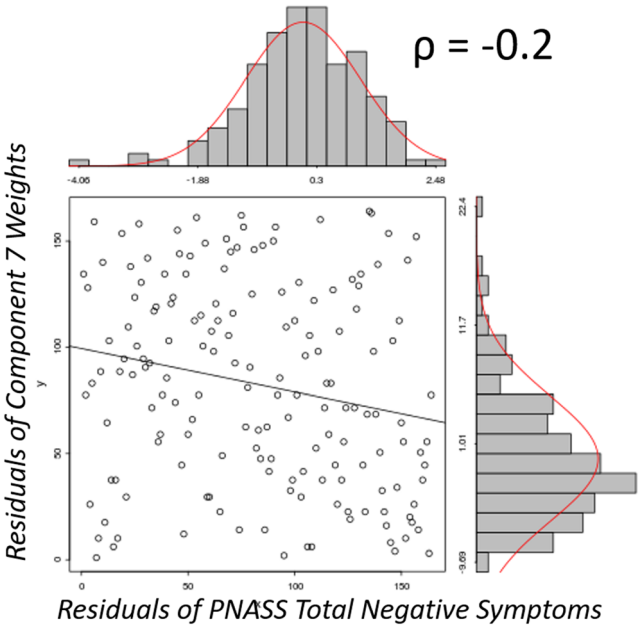

FIGURE 5 Spearman rank correlation between the residuals of PNASS total negative symptom scores and laterality component 7 weights when accounting for differences in acquisition sites. The line is the linear correlation between ranks for residuals of component 7 weights and total negative symptoms from the PNASS. The histograms on the x and y axis illustrate the (skewed) distributions of the residuals of the variables accounting for data acquisition site

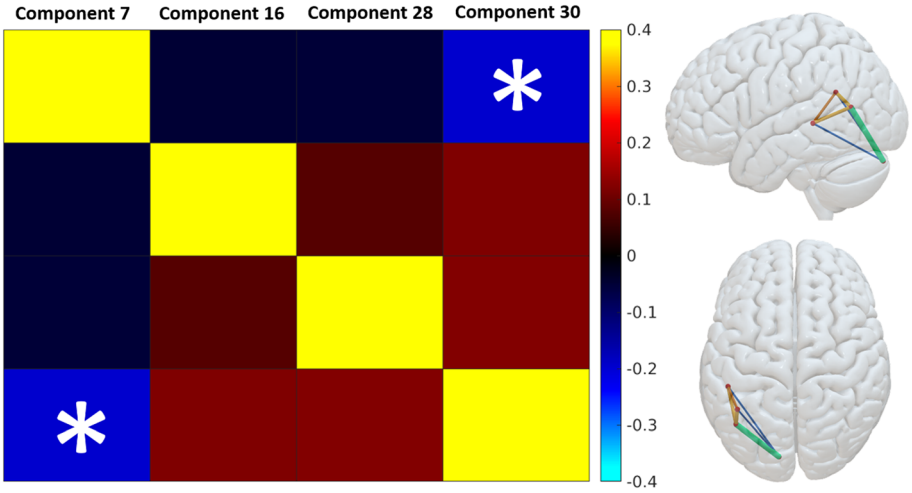

FIGURE 6 Structural FNC matrix of components 7, 16, 28 and 30 (left). Nodal illustration of all four components, with structural connectivity between component 7 and 30 (* on matrix and cyan on nodal illustration) statistically significant following a Holm correction for multiple comparisons

results. As a demonstration of the utility of SBL, the technique was applied to a cohort of SZ participants relative to controls. This comparison revealed alterations in multiple covarying networks including left, middle and superior temporal regions, and the planum temporale consistent with extensive SZ literature.[2–6,8–10,13–23,63–72] An exception to this trend is altered subcortical asymmetry in schizophrenia from meta-analyses such as performed by Okada et al,[93] whose 2016 meta-analysis of structural laterality of subcortical regions from 2564 datasets across 78 studies identified significant differences in LI specific to the globus pallidus and no other subcortical regions. However, it should be noted that even when effect size-weighted meta-analytic methods are considered, meta-analyses may be influenced by publication bias, where effects within the literature which do not fail to reject the null hypothesis are not reported.[94–96] While not 100% reflective of the literature, tools are available to provide estimates of such biases.[96–100] In addition, it is important to keep in mind that atlas-based and data-driven ROIs have different advantages. To the degree an entire region is changing in volume, an ROI approach may provide enhanced sensitivity. However, if changes are variable across the ROI, are more focal, or vary across individuals, a data-driven approach will likely perform better under these circumstances. Given these possibilities and the relatively small effect sizes reported for CON versus SZ across studies (≤0.3, see supplementary table 10 in Okada et al[93]), subcortical alterations in laterality may have been negligible to a degree that they were not detected in SBL. It will be important to leverage multiple analytic approaches to capture changes via a pluralistic lens.

The results of this pilot SBL approach are the first, to our knowledge, to identify laterality differences within paired, but discrete, regions of the temporal lobe. The covariation of separate subregions within the temporal lobe in the real data may reflect separate sources discrete to the numerous functions recruited by the temporal lobes, and relationships these regions have with laterality alterations present in SZ compared with

CON participants. While additional work will be required to validate such brain/behavior relationships, this highlights the unique advantage of SBL over traditional approaches, in that discrete covarying networks are identified.

The earliest work by Wernicke implied that these regions were critical to language, which has since expanded to include many aspects of social cognition.[101,102] Previous work has suggested left anterior portions of the STG/MTG are key for language integration, while posterior STG/MTG are key to speech production and other cognitive functions in a graded manner.[101,102] It is entirely possible that components 16, 28 and 30 were separated based on this graded topology, although future studies will be needed to evaluate this hypothesis. Additional behavioral data specific to each language domain (eg, word generation, integration, phoneme clustering) would be necessary to probe this hypothesis. Previous literature and the results presented here would suggest alterations in left-lateralized regions specific to language may explain some of the negative symptoms of schizophrenia, however, the significant relationship between negative PANSS scores and the cerebellum may hint towards a rarely explored avenue of research in SZ.

The cerebellum has similarly been linked to language and social cognition. Right cerebellar resection from cranial fossa tumors produce deficits in complex language tasks and speech alterations ranging from mutism to dysarthria.[103–105] These symptoms are not unlike some of the negative symptoms described in the PANSS.[89] Previous work has suggested alterations within Purkinje cells and associated proteins within the cerebellum are altered in individuals with schizophrenia, but the impact is not fully understood.[106,107] Furthermore, most of these experiments have focused on motor function, a fraction of which is measured by PANSS negative symptom scores. Diffusion weighted imaging tractography studies in humans suggest physical connections are present between the cerebellum and contralateral MTG.[108] Additionally, previous work has also found VBM-based reductions in white matter within temporal regions in SZ.[109] Gray matter volume SNC results between the cerebellum and temporal regions may reflect alterations within this pathway.

While this theory is bolstered by the significant negative relationship between negative PANSS symptom scores and the cerebellar component, the relatively small effect sizes for diagnosis for the components ($_p\acute{\omega}^2$ = 0.012-0.035) suggests the effect may not be very strong within the modality of structural MRI. We argue that future work using multimodal difference maps (eg, diffusion anisotropy, fMRI) with fusion approaches such as joint ICA or independent vector analysis (IVA) may be able to capture a structural and functional interaction(s) within SZ and other populations.

The SBL approach has advantages over traditional ROI- and voxel-based approaches in that it can identify covarying spatial laterality patterns, possesses much greater statistical power regarding the number of multiple comparison corrections both for ICA components and a reduction in the total voxels tested, and is relatively easy to implement within the framework of existing ICA tools. SBL component weights appear to reflect differences in hemispheric differences scores (translating to laterality), which can serve as a useful tool for post hoc volumetric analyses at the ROI or voxel level. Further work will be required to evaluate the SBL approach for assessing laterality, but these factors suggest the SBL approach is a promising direction for studying brain laterality.

4.1 | Limitations

While the SBL approach does provide the advantage of localization to covarying regions across hemispheres, interpreting the direction of alterations requires more refinement. In the mirror image, negative values are indicative of greater volume in the right hemisphere, positive values in the left hemisphere, and relative differences of 0 indicate a lack of laterality. The ICA implementation used for the SBL approach will flip signs when estimating components, as demonstrated in Figures 4A and 3B. As such, component weights (positive or negative) must be carefully calibrated to represent the direction of lateralization. This is especially important regarding the cerebellum, as the contralateral connections with the cortex may affect the interpretation of the results. As stated in the discussion, the authors have suggested that multi-modal data fusion analyses[110] may be able to provide additional information regarding the validity/utility of these effects, and this research venue is recommended prior to any definitive conclusions.

ACKNOWLEDGEMENTS

This project was supported by National Institute of Biomedical Imaging and Bioengineering grants R01EB020407, R01EB006841, National Institute of General Medical Sciences grants P20GM103472 and P30GM122734, National Institute of Mental Health grant R01MH094524, and National Science Foundation grant number 1539067. We acknowledge the developers of the *Seaborn* package in Python, the *effsize*, *fifer*, *ppcor*, *sjstats*, in *R*, and the *papaya* image viewer at University of Texas Health, San Antonio for data analysis and visualization.

FUNDING INFORMATION

National Institute of Health (NIH) grants: R01EB020407, R01EB006841, R01MH094524, P20GM103472 and P30GM122734; National Science Foundation (NSF) grant no. 1539067.

ORCID

Thomas P. DeRamus https://orcid.org/0000-0002-5774-2297

REFERENCES

1. Sumich A, Chitnis XA, Fannon DG, et al. Unreality symptoms and volumetric measures of Heschl's gyrus and planum temporal in first-episode psychosis. *Biol Psychiatry*. 2005;57(8):947-950.
2. Ratnanather JT, Poynton CB, Pisano DV, et al. Morphometry of superior temporal gyrus and planum temporale in schizophrenia and psychotic bipolar disorder. *Schizophr Res*. 2013;150(2-3):476-483.
3. Kasai K, Shenton ME, Salisbury DF, et al. Progressive decrease of left superior temporal gyrus gray matter volume in patients with first-episode schizophrenia. *Am J Psychiatry*. 2003;160(1):156-164.
4. Rajarethinam RP, DeQuardo JR, Nalepa R, Tandon R. Superior temporal gyrus in schizophrenia: a volumetric magnetic resonance imaging study. *Schizophr Res*. 2000;41(2):303-312.
5. Gupta CN, Calhoun VD, Rachakonda S, et al. Patterns of gray matter abnormalities in schizophrenia based on an international mega-analysis. *Schizophr Bull*. 2015;41(5):1133-1142.
6. Hirayasu Y, McCarley R, Salisbury DF, et al. Planum temporale and Heschl gyrus volume reduction in schizophrenia: a magnetic resonance imaging study of first-episode patients. *Arch Gen Psychiatry*. 2000;57(7):692-699.
7. Loeber RT, Cintron CM, Yurgelun-Todd DA. Morphometry of individual cerebellar lobules in schizophrenia. *Am J Psychiatry*. 2001;158(6):952-954.
8. Yamasaki S, Yamasue H, Abe O, et al. Reduced planum temporale volume and delusional behaviour in patients with schizophrenia. *Eur Arch Psychiatry Clin Neurosci*. 2007;257(6):318-324.
9. Spalthoff R, Gaser C, Nenadić I. Altered gyrification in schizophrenia and its relation to other morphometric markers. *Schizophr Res*. 2018;202:195-202.
10. Honea R, Crow TJ, Passingham D, Mackay CE. Regional deficits in brain volume in schizophrenia: a meta-analysis of voxel-based morphometry studies. *Am J Psychiatry*. 2005;162(12):2233-2245.
11. Sommer I, Ramsey N, Kahn R, Aleman A, Bouma A. Handedness, language lateralisation and anatomical asymmetry in schizophrenia: meta-analysis. *Br J Psychiatry*. 2001;178:344-351.
12. Kawasaki Y, Suzuki M, Takahashi T, et al. Anomalous cerebral asymmetry in patients with schizophrenia demonstrated by voxel-based morphometry. *Biol Psychiatry*. 2008;63(8):793-800.
13. Barta PE, Pearlson GD, Brill LB 2nd, et al. Planum temporale asymmetry reversal in schizophrenia: replication and relationship to gray matter abnormalities. *Am J Psychiatry*. 1997;154(5):661-667.
14. Bleich-Cohen M, Hendler T, Kotler M, Strous RD. Reduced language lateralization in first-episode schizophrenia: an fMRI index of functional asymmetry. *Psychiatry Res*. 2009;171(2):82-93.
15. Discussion. *Trends Neurosci*. 1997;20(8):339-343.
16. Crow TJ, Ball J, Bloom SR, et al. Schizophrenia as an anomaly of development of cerebral asymmetry. A postmortem study and a proposal concerning the genetic basis of the disease. *Arch Gen Psychiatry*. 1989;46(12):1145-1150.
17. Falkai P, Bogerts B, Schneider T, et al. Disturbed planum temporale asymmetry in schizophrenia. A quantitative post-mortem study. *Schizophr Res*. 1995;14(2):161-176.
18. Kleinschmidt A, Falkai P, Huang Y, Schneider T, Fürst G, Steinmetz H. In vivo morphometry of planum temporale asymmetry in first-episode schizophrenia. *Schizophr Res*. 1994;12(1):9-18.
19. Oertel-Knöchel V, Linden DEJ. Cerebral asymmetry in schizophrenia. *Neuroscientist*. 2011;17(5):456-467.
20. Ragland JD, Gur RE, Klimas BC, McGrady N, Gur RC. Neuropsychological laterality indices of schizophrenia: interactions with gender. *Schizophr Bull*. 1999;25(1):79-89.
21. Rossi A, Serio A, Stratta P, et al. Planum temporale asymmetry and thought disorder in schizophrenia. *Schizophr Res*. 1994;12(1):1-7.
22. Saugstad LF. A lack of cerebral lateralization in schizophrenia is within the normal variation in brain maturation but indicates late, slow maturation. *Schizophr Res*. 1999;39(3):183-196.
23. Shenton ME, Kikinis R, Jolesz FA, et al. Abnormalities of the left temporal lobe and thought disorded in schizophrenia. A quantitative magnetic resonance imaging study. *New Engl J Med*. 1992;327(9):604-612.
24. Hinke RM, Hu X, Stillman AE, et al. Functional magnetic resonance imaging of Broca's area during internal speech. *Neuroreport*. 1993;4(6):675-678.
25. Desmond JE, Sum JM, Wagner AD, et al. Functional MRI measurement of language lateralization in Wada-tested patients. *Brain*. 1995;118(Pt 6):1411-1419.
26. Binder JR, Swanson SJ, Hammeke TA, et al. Determination of language dominance using functional MRI: a comparison with the Wada test. *Neurology*. 1996;46(4):978-984.
27. Seghier ML. Laterality index in functional MRI: methodological issues. *Magn Reson Imaging*. 2008;26(5):594-601.
28. Stevens MC, Calhoun VD, Kiehl KA. Hemispheric differences in hemodynamics elicited by auditory oddball stimuli. *Neuroimage*. 2005;26(3):782-792.
29. Wilke M, Lidzba K. LI-tool: a new toolbox to assess lateralization in functional MR-data. *J Neurosci Methods*. 2007;163(1):128-136.
30. Benson RR, FitzGerald D, LeSueur L, et al. Language dominance determined by whole brain functional MRI in patients with brain lesions. *Neurology*. 1999;52(4):798-809.
31. Adcock JE, Wise RG, Oxbury JM, Oxbury SM, Matthews PM. Quantitative fMRI assessment of the differences in lateralization of language-related brain activation in patients with temporal lobe epilepsy. *Neuroimage*. 2003;18(2):423-438.
32. Bethmann A, Tempelmann C, De Bleser R, Scheich H, Brechmann A. Determining language laterality by fMRI and dichotic listening. *Brain Res*. 2007;1133(1):145-157.
33. Fernandes MA, Smith ML, Logan W, Crawley A, McAndrews MP. Comparing language lateralization determined by dichotic listening and fMRI activation in frontal and temporal lobes in children with epilepsy. *Brain Lang*. 2006;96(1):106-114.
34. Harrington GS, Buonocore MH, Farias ST. Intrasubject reproducibility of functional MR imaging activation in language tasks. *Am J Neuroradiol*. 2006;27(4):938-944.
35. Fernández G, de Greiff A, von Oertzen J, et al. Language mapping in less than 15 minutes: real-time functional MRI during routine clinical investigation. *Neuroimage*. 2001;14(3):585-594.
36. Fernández G, Specht K, Weis S, et al. Intrasubject reproducibility of presurgical language lateralization and mapping using fMRI. *Neurology*. 2003;60(6):969-975.

37. Branco DM, Suarez RO, Whalen S, et al. Functional MRI of memory in the hippocampus: Laterality indices may be more meaningful if calculated from whole voxel distributions. *Neuroimage*. 2006;32(2):592-602.
38. Wilke M, Schmithorst VJ. A combined bootstrap/histogram analysis approach for computing a lateralization index from neuroimaging data. *Neuroimage*. 2006;33(2):522-530.
39. Chlebus P, Mikl M, Brázdil M, Pazourková M, Krupa P, Rektor I. fMRI evaluation of hemispheric language dominance using various methods of laterality index calculation. *Exp Brain Res*. 2007;179(3):365-374.
40. Jansen A, Menke R, Sommer J, et al. The assessment of hemispheric lateralization in functional MRI--robustness and reproducibility. *Neuroimage*. 2006;33(1):204-217.
41. Karbe H, Thiel A, Weber-Luxenburger G, Herholz K, Kessler J, Heiss WD. Brain plasticity in poststroke aphasia: what is the contribution of the right hemisphere? *Brain Lang*. 1998;64(2):215-230.
42. Hubrich-Ungureanu P, Kaemmerer N, Henn FA, Braus DF. Lateralized organization of the cerebellum in a silent verbal fluency task: a functional magnetic resonance imaging study in healthy volunteers. *Neurosci Lett*. 2002;319(2):91-94.
43. Krainik A, Duffau H, Capelle L, et al. Role of the healthy hemisphere in recovery after resection of the supplementary motor area. *Neurology*. 2004;62(8):1323-1332.
44. Fischl B, van der Kouwe A, Destrieux C, et al. Automatically parcellating the human cerebral cortex. *Cereb Cortex*. 2004;14(1):11-22.
45. Desikan RS, Ségonne F, Fischl B, et al. An automated labeling system for subdividing the human cerebral cortex on MRI scans into gyral based regions of interest. *Neuroimage*. 2006;31(3):968-980.
46. Dale AM, Fischl B, Sereno MI. Cortical surface-based analysis. I Segmentation and surface reconstruction. *Neuroimage*. 1999;9(2):179-194.
47. Fischl B, Sereno MI, Dale AM. Cortical surface-based analysis. II: Inflation, flattening, and a surface-based coordinate system. *Neuroimage*. 1999;9(2):195-207.
48. Fischl B, Dale AM. Measuring the thickness of the human cerebral cortex from magnetic resonance images. *Proc Natl Acad Sci U S A*. 2000;97(20):11050-11055.
49. Fischl B, Salat DH, Busa E, et al. Whole brain segmentation: automated labeling of neuroanatomical structures in the human brain. *Neuron*. 2002;33(3):341-355.
50. Fischl B, Sereno MI, Tootell RB, Dale AM. High-resolution intersubject averaging and a coordinate system for the cortical surface. *Hum Brain Mapp*. 1999;8(4):272-284.
51. Fischl B, Liu A, Dale AM. Automated manifold surgery: constructing geometrically accurate and topologically correct models of the human cerebral cortex. *IEEE Trans Med Imaging*. 2001;20(1):70-80.
52. Poldrack RA. Region of interest analysis for fMRI. *Soc Cogn Affect Neurosci*. 2007;2(1):67-70.
53. Tong Y, Chen Q, Nichols TE, et al. Seeking optimal region-of-interest (ROI) single-value summary measures for fMRI studies in imaging genetics. *PLoS ONE*. 2016;11(3):e0151391.
54. Scarpazza C, Tognin S, Frisciata S, Sartori G, Mechelli A. False positive rates in Voxel-based Morphometry studies of the human brain: should we be worried? *Neurosci Biobehav Rev*. 2015;52:49-55.
55. Patriquin MA, DeRamus T, Libero LE, Laird A, Kana RK. Neuroanatomical and neurofunctional markers of social cognition in autism spectrum disorder. *Human brain mapping*. 2016;37(11):3957-3978.
56. Dickie DA, Mikhael S, Job DE, Wardlaw JM, Laidlaw DH, Bastin ME. Permutation and parametric tests for effect sizes in voxel-based morphometry of gray matter volume in brain structural MRI. *Magn Reson Imaging*. 2015;33(10):1299-1305.
57. Mechelli A, Price C, Friston K, Ashburner J. Voxel-based morphometry of the human brain: methods and applications. *Curr Med Imaging Rev*. 2005;1:105-113.
58. Jones DK, Symms MR, Cercignani M, Howard RJ. The effect of filter size on VBM analyses of DT-MRI data. *Neuroimage*. 2005;26(2):546-554.
59. Senjem ML, Gunter JL, Shiung MM, Petersen RC, Jack CR. Comparison of different methodological implementations of voxel-based morphometry in neurodegenerative disease. *Neuroimage*. 2005;26:600-608.
60. Xu L, Groth KM, Pearlson G, Schretlen DJ, Calhoun VD. Source-based morphometry: the use of independent component analysis to identify gray matter differences with application to schizophrenia. *Hum Brain Mapp*. 2009;30(3):711-724.
61. Keator DB, Grethe JS, Marcus D, et al. A national human neuroimaging collaboratory enabled by the Biomedical Informatics Research Network (BIRN). *IEEE Trans Inf Technol Biomed*. 2008;12(2):162-172.
62. Keator DB, van Erp T, Turner JA, et al. The function biomedical informatics research network data repository. *Neuroimage*. 2016;124(Pt B):1074-1079.
63. Sommer IE, Ramsey NF, Kahn RS. Language lateralization in schizophrenia, an fMRI study. *Schizophr Res*. 2001;52(1-2):57-67.
64. Falkai P, Bogerts B, Greve B, et al. Loss of sylvian fissure asymmetry in schizophrenia. *Schizophr Res*. 1992;7(1):23-32.
65. Crow TJ. Cerebral asymmetry and the lateralization of language: core deficits in schizophrenia as pointers to the gene. *Curr Opin Psychiatry*. 2004;17:97-106.
66. Kasai K, Shenton ME, Salisbury DF, et al. Progressive decrease of left Heschl gyrus and planum temporale gray matter volume in first-episode schizophrenia: a longitudinal magnetic resonance imaging study. *Arch Gen Psychiatry*. 2003;60(8):766-775.
67. Kwon JS, McCarley R, Hirayasu Y, et al. Left planum temporale volume reduction in schizophrenia. *Arch Gen Psychiatry*. 1999;56(2):142-148.
68. Kong L, Bachmann S, Thomann PA, Essig M, Schröder J. Neurological soft signs and gray matter changes: a longitudinal analysis in first-episode schizophrenia. *Schizophr Res*. 2012;134(1):27-32.
69. Petty RG, Barta PE, Pearlson GD, et al. Reversal of asymmetry of the planum temporale in schizophrenia. *Am J Psychiatry*. 1995;152(5):715-721.
70. Glahn DC, Laird AR, Ellison-Wright I, et al. Meta-analysis of gray matter anomalies in schizophrenia: application of anatomic likelihood estimation and network analysis. *Biol Psychiatry*. 2008;64(9):774-781.
71. Royer C, Delcroix N, Leroux E, et al. Functional and structural brain asymmetries in patients with schizophrenia and bipolar disorders. *Schizophr Res*. 2015;161(2-3):210-214.
72. Shapleske J, Rossell SL, Woodruff PW, David AS. The planum temporale: a systematic, quantitative review of its structural, functional and clinical significance. *Brain Res Brain Res Rev*. 1999;29(1):26-49.

73. Calhoun VD, Adali T, Pearlson GD, Pekar JJ. A method for making group inferences from functional MRI data using independent component analysis. *Hum Brain Mapp*. 2001;14(3):140-151.
74. Oldfield RC. The assessment and analysis of handedness: the Edinburgh inventory. *Neuropsychologia*. 1971;9(1):97-113.
75. Esteban O, Birman D, Schaer M, Koyejo OO, Poldrack RA, Gorgolewski KJ. MRIQC: Advancing the automatic prediction of image quality in MRI from unseen sites. *PLoS ONE*. 2017;12(9):e0184661.
76. Schuch FB, Vancampfort D, Richards J, Rosenbaum S, Ward PB, Stubbs B. Exercise as a treatment for depression: A meta-analysis adjusting for publication bias. *J Psychiatr Res*. 2016;77:42-51.
77. Yannakopoulou K, Jicsinszky L, Aggelidou C, et al. Symmetry requirements for effective blocking of pore-forming toxins: comparative study with alpha-, beta-, and gamma-cyclodextrin derivatives. *Antimicrob Agents Chemother*. 2011;55(7):3594-3597.
78. Godinho R, Domingues V, Crespo EG, Ferrand N. Extensive intraspecific polymorphism detected by SSCP at the nuclear C-mos gene in the endemic Iberian lizard Lacerta schreiberi. *Mol Ecol*. 2006;15(3):731-738.
79. Smith SM, Jenkinson M, Woolrich MW, et al. Advances in functional and structural MR image analysis and implementation as FSL. *Neuroimage*. 2004;23(Suppl 1):S208-S219.
80. Jenkinson M, Beckmann CF, Behrens TEJ, Woolrich MW, Smith SM. FSL. *Neuroimage*. 2012;62(2):782-790.
81. Avants BB, Tustison N, Song G. Advanced Normalization Tools (ANTS). *Insight J*. 2009;2:1-35.
82. Avants BB, Tustison NJ, Wu J, Cook PA, Gee JC. An open source multivariate framework for n-tissue segmentation with evaluation on public data. *Neuroinformatics*. 2011;9(4):381-400.
83. Cox RW. AFNI: software for analysis and visualization of functional magnetic resonance neuroimages. *Comput Biomed Res*. 1996;29(3):162-173.
84. Akaike H. A new look at the statistical model identification. *IEEE transactions on automatic control*. 197419(6):716-723.
85. Li X-L, Adali T. Blind spatiotemporal separation of second and/or higher-order correlated sources by entropy rate minimization. In *2010 IEEE International Conference on Acoustics, Speech and Signal Processing*. IEEE;2010:1934-1937.
86. Li X-L, Adali T. Independent component analysis by entropy bound minimization. *IEEE Trans Signal Process*. 2010;58:5151-5164.
87. Du W, Li H, Li X-L, Calhoun VD, Adali T. ICA of fMRI data: Performance of three ICA algorithms and the importance of taking correlation information into account. In *2011 IEEE International Symposium on Biomedical Imaging: From Nano to Macro*. IEEE; 2011:1573-1576.
88. Benjamini Y, Drai D, Elmer G, Kafkafi N, Golani I. Controlling the false discovery rate in behavior genetics research. *Behav Brain Res*. 2001;125(1-2):279-284.
89. Kay SR, Fiszbein A, Opler LA. The positive and negative syndrome scale (PANSS) for schizophrenia. *Schizophr Bull*. 1987;13(2):261-276.
90. Hirata M. Inhibitory effects of antihistamines and antiserotonins on the bone marrow reactions produced by *Escherichia coli* endotoxin in mice. *J Infect Dis*. 1975;132(6):611-616.
91. Wilcoxon F. Individual comparisons of grouped data by ranking methods. *J Econ Entomol*. 1946;39(2):269-270.
92. R Core Team. R: A Language and Environment for Statistical Computing.
93. Okada N, Fukunaga M, Yamashita F, et al. Abnormal asymmetries in subcortical brain volume in schizophrenia. *Mol Psychiatry*. 2016;21(10):1460-1466.
94. Han B, Eskin E. Random-effects model aimed at discovering associations in meta-analysis of genome-wide association studies. *Am J Hum Genet*. 2011;88(5):586-598.
95. Lakens D, Hilgard J, Staaks J. On the reproducibility of meta-analyses: six practical recommendations. *BMC Psychol*. 2016;4(1):1-10.
96. Samartsidis P, Montagna S, Laird AR, Fox PT, Johnson TD, Nichols TE. Estimating the number of missing experiments in a neuroimaging meta-analysis. *bioRxiv*. 2017;225425.
97. Simonsohn U, Nelson LD, Simmons J. P-curve and effect size: correcting for publication bias using only significant results. *Perspect Psychol Sci*. 2014;9(6):666-681.
98. Simonsohn U, Nelson LD, Simmons JP. P-curve won't do your laundry, but it will distinguish replicable from non-replicable findings in observational research: Comment on Bruns & Ioannidis (2016). *PLoS ONE*. 2019;14(3):e0213454.
99. Simonsohn U, Nelson LD, Simmons JP. P-curve: a key to the file-drawer. *J Exp Psychol Gen*. 2014;143(2):534-547.
100. Simonsohn U, Simmons JP, Nelson LD. Better P-curves: Making P-curve analysis more robust to errors, fraud, and ambitious P-hacking, a Reply to Ulrich and Miller (2015). *J Exp Psychol Gen*. 2015;144(6):1146-1152.
101. DeWitt I, Rauschecker JP. Phoneme and word recognition in the auditory ventral stream. *Proc Natl Acad Sci U S A*. 2012;109(8):E505-E514.
102. DeWitt I, Rauschecker JP. Wernicke's area revisited: parallel streams and word processing. *Brain Lang*. 2013;127(2):181-191.
103. Pollack IF, Polinko P, Albright AL, Towbin R, Fitz C. Mutism and pseudobulbar symptoms after resection of posterior fossa tumors in children: incidence and pathophysiology. *Neurosurgery*. 1995;37(5):885-893.
104. Poggi G, Liscio M, Galbiati S, et al. Brain tumors in children and adolescents: cognitive and psychological disorders at different ages. *Psychooncology*. 2005;14(5):386-395.
105. Riva D, Giorgi C. The cerebellum contributes to higher functions during development: evidence from a series of children surgically treated for posterior fossa tumours. *Brain*. 2000;123(Pt 5):1051-1061.
106. Eastwood SL, Cotter D, Harrison PJ. Cerebellar synaptic protein expression in schizophrenia. *Neuroscience*. 2001;105(1):219-229.
107. Andreasen NC, Pierson R. The role of the cerebellum in schizophrenia. *Biol Psychiatry*. 2008;64(2):81-88.
108. Sokolov AA, Erb M, Grodd W, Pavlova MA. Structural loop between the cerebellum and the superior temporal sulcus: evidence from diffusion tensor imaging. *Cereb Cortex*. 2014;24(3):626-632.
109. Ellison-Wright I, Bullmore E. Meta-analysis of diffusion tensor imaging studies in schizophrenia. *Schizophr Res*. 2009;108:3-10.
110. Calhoun VD, Sui J. Multimodal fusion of brain imaging data: A key to finding the missing link(s) in complex mental illness. *Biol Psychiatry Cogn Neurosci Neuroimaging*. 2016;1(3):230-244.

SUPPORTING INFORMATION

Additional supporting information may be found online in the Supporting Information section at the end of this article.

How to cite this article: DeRamus TP, Silva RF, Iraji A, et al. Covarying structural alterations in laterality of the temporal lobe in schizophrenia: A case for source-based laterality. *NMR in Biomedicine*. 2020;33:e4294. https://doi.org/10.1002/nbm.4294